Active Control and Stability Analysis of Flexible Structures using Nonlinear Proof-Mass Actuators

L. I. Wilmshurst[1], M. Ghandchi-Tehrani[2], S. J. Elliott[3]
[1]Signal Processing and Control Group, Institute of Sound and Vibration Research, University of Southampton, Mr. Laurence Wilmshurst, 3043 Southampton, UK
[2]Signal Processing and Control Group, Institute of Sound and Vibration Research, University of Southampton, Dr. Maryam Ghandchi-Tehrani, 3067 Southampton, UK
[3]Signal Processing and Control Group, Institute of Sound and Vibration Research, University of Southampton, Prof. Stephen Elliott, 3059 Southampton, UK
email: lw5e10@soton.ac.uk, M.Ghandchi-Tehrani@soton.ac.uk, S.J.Elliott@soton.ac.uk

ABSTRACT: Proof-mass actuators are highly advantageous for active control of structures, due to their large force-to-weight ratio and their ability to provide inertia without a ground reference. These devices comprise a proof-mass suspended in a magnetic field that is accelerated by an input voltage, in order to provide a reaction force on the actuator casing and the structure itself. However, if the input voltage is large, the proof-mass will hit the end-stops, thereby imparting large shocks to the structure that may destabilise the closed-loop system.

To ensure that the closed-loop system is asymptotically stable, a control law that counteracts the destabilising effects of stroke saturation must be designed. First, a numerical study is conduced, where a dynamic model of a Micromega IA-01 proof-mass actuator is coupled to a flexible structure in a collocated pure-gain velocity-feedback closed-loop configuration. Using Lyapunov's direct method, it is shown that stroke saturation greatly reduces the closed-loop stability margin, due to large increases in the kinetic energy as the proof-mass moves from one end stop to the other. Finally, an alternative on-off feedback control strategy is briefly investigated, and its merits and drawbacks are discussed.

KEY WORDS: Active control, proof-mass actuator, Lyapunov stability.

1 INTRODUCTION

The ever-increasing demand for smart, flexible structures in recent times has necessitated the use of active control as a means of damage detection and limiting structural vibration. Passive control methods typically add mass to the structure, which conflicts with the requirements for lightness and flexibility, and is not usually effective at low frequencies. In order to apply active control to a structure, its velocity or displacement is fed back to a collocated actuator to generate a control force, such that the effective stiffness or damping of the closed-loop system is increased in relation to the open-loop system [1].

Proof-mass actuators, which generate a control force by means of accelerating an inertial mass in response to an input voltage, are highly advantageous for this purpose, due to their ability to provide a large inertial force without a ground reference [2]. However, one significant drawback of these actuators is that the displacement of the proof-mass is limited by the actuator stroke length; therefore, if the input voltage is large, the proof-mass will collide with the end stops and the displacement amplitude is saturated [3]. This phenomenon is known as stroke saturation.

In general, stroke saturation is detrimental to the performance of the closed-loop system, for a number of reasons. Firstly, large impulses are generated from the collisions of the proof-mass and the end stops, which are transmitted to the structure and may result in damage. Secondly, it limits the effect of active control. Thirdly, it has been observed experimentally that stoke saturation can destabilise the closed-loop system [4]. This is problematic for systems that are frequently subjected to large disturbances, such as seismic excitation, and so it is desirable that the closed-loop system remains stable for large inputs [5]. Furthermore, destabilization is particularly severe in MIMO systems that utilise multiple actuators, since instability in one loop will induce instability in the other loops [6]

In this study, the stability of a nonlinear proof-mass actuator coupled to a linear structure in a two-degree-of-freedom closed-loop configuration is investigated. Recently, Wilmshurst *et al.* [7] modelled a proof-mass actuator [8] using a lumped parameter system, based on experimental measurements and previous work by Baumann and Elliott [4]. It was found that a piecewise linear stiffness model was able to reasonably emulate the dynamics of a stoke-saturated actuator, which were obtained using experimental measurements. Section 2 covers the theoretical aspects of the study, and shows that the closed-loop system exhibits limit-cycle oscillations, even if the Nyquist gain and phase margins are not exceeded. Section 3 describes the application of Lyapunov's direct method to the nonlinear system, where it is found that the instabilities can be related to a sequence of events that results in a large increase in the kinetic energy of the proof-mass as it moves from one end stop to the other. Section 4 briefly investigates the effect of on-off feedback control on the overall closed-loop stability. Conclusions and future work are stated in Section 5.

2 THEORY

The general state-space equation for the nonlinear actuator dynamics is,

$$\dot{\mathbf{x}} = \mathbf{f}(\mathbf{x}) + \mathbf{B}f_p \tag{1}$$

where $\mathbf{x} = [x_p \ \dot{x}_p]^T$ is the actuator displacement and velocity respectively, $\mathbf{f(x)}$ represents the nonlinear system equations, $\mathbf{B}$ is the input matrix and f_p is the primary input signal. The linear piecewise model obtained in [7] can be written as,

$$\mathbf{f(x)} = \begin{bmatrix} x_p \\ \frac{-1}{m_p}(k_p x_p + c_p \dot{x}_p + f_{sat}) \end{bmatrix}, \quad \mathbf{B} = \begin{bmatrix} 0 \\ \frac{g}{m_p} \end{bmatrix} \tag{2}$$

where,

$$f_{sat} = \begin{cases} k_{sat}(x_p - d) & x_p > d \\ 0 & |x_p| < d \\ k_{sat}(x_p + d) & x_p < -d \end{cases} \tag{3}$$

Here, m_p is the mass of the internal proof-mass, k_p and c_p are the stiffness and damping terms of the actuator suspension, k_{sat} is the equivalent stiffness associated with stroke saturation, d is the stroke length, and g is the actuator gain. By incorporating this model in the actuator-structure configuration, as shown in Figure 1, the closed-loop system dynamics can be described using,

$$\dot{\mathbf{x}} = \mathbf{f(x)} + \mathbf{B_p} f_p + \mathbf{B_s} f_s \tag{4}$$

where $\mathbf{x} = [x_s \ \dot{x}_s \ x_p \ \dot{x}_p]^T$ represents the respective displacements and velocities of the structure and actuator, $\mathbf{f(x)}$ is a vector of nonlinear equations that describes the open-loop dynamics, $\mathbf{B_p}, \mathbf{B_s}$ are the input and control matrices respectively, and f_p, f_s are the input force and control signal respectively.

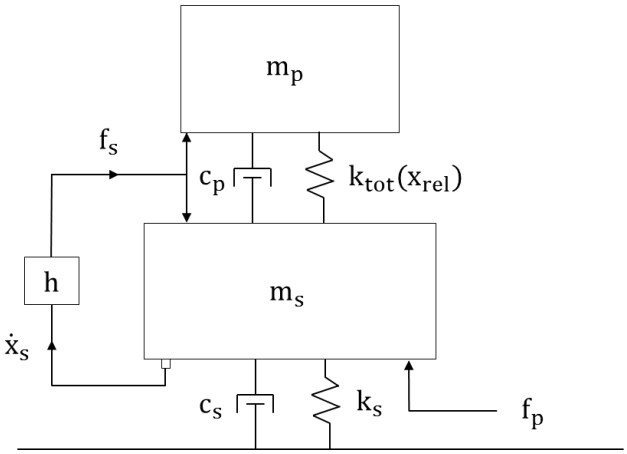

Figure 1. Actuator-structure configuration.

From Figure 1, the closed-loop dynamics can be written as,

$$\mathbf{f(x)} = \begin{bmatrix} x_s \\ x_p \\ \frac{-1}{m_s}(k_s x_s + (c_p + c_s)\dot{x}_s + k_{tot}(x_{tot}) - c_p \dot{x}_p) \\ \frac{-1}{m_p}(k_{tot}(x_{tot}) + c_p \dot{x}_p - c_p \dot{x}_s) \end{bmatrix}$$

$$\mathbf{B_p} = \begin{bmatrix} 0 \\ 0 \\ \frac{1}{m_s} \\ 0 \end{bmatrix}, \quad \mathbf{B_s} = \begin{bmatrix} 0 \\ 0 \\ \frac{-g}{m_s} \\ \frac{g}{m_p} \end{bmatrix} \tag{5}$$

where k_s, c_s are the stiffness and damping coefficients of the structure, $k_{tot}(x_{tot})$ is the total nonlinear stiffness of the proof-mass suspension, and $x_{rel} = x_p - x_s$ is the relative displacement between the proof-mass and the structural mass. Since the output structural velocity $\dot{x}_s$ is fed back to the system, the control signal f_s is,

$$f_s = -h\mathbf{C_v}\mathbf{x}, \quad \mathbf{C_v} = [0 \ \ 0 \ \ 1 \ \ 0] \tag{6}$$

where h is the feedback control gain. By incorporating the control force into $\mathbf{f(x)}$, a new set of nonlinear equations $\mathbf{g(x)}$ is obtained that describes the closed-loop dynamics,

$$\dot{\mathbf{x}} = \mathbf{g(x)} + \mathbf{B_p} f_p \tag{7}$$

where

$$\mathbf{g(x)} = \begin{bmatrix} x_s \\ x_p \\ \frac{-1}{m_s}(k_s x_s + c_v \dot{x}_s + k_{tot}(x_s, x_p) - c_p \dot{x}_p) \\ \frac{-1}{m_p}(k_{tot}(x_s, x_p) + c_p \dot{x}_p - (c_p + h)\dot{x}_s) \end{bmatrix} \tag{8}$$

c_v being $c_s + c_p + h$. By comparing Eq. (8) with Eq. (5), it is apparent that the control signal has the effect of increasing the damping of the structure whilst increasing the effective negative damping of the proof-mass. The result is that the structural vibration will decrease at the expense of the proof-mass vibration, which may destabilize the closed-loop system if the control gain is too large.

Provided that the relative displacement is small ($|x_{rel}| < d$), the open-loop dynamics can be described using the second-order realization,

$$\mathbf{M}\ddot{\mathbf{q}} + \mathbf{C}\dot{\mathbf{q}} + \mathbf{K}\mathbf{q} = \mathbf{f} \tag{9}$$

where,

$$\mathbf{M} = \begin{bmatrix} m_s & 0 \\ 0 & m_p \end{bmatrix}, \mathbf{C} = \begin{bmatrix} c_s + c_p & -c_p \\ -c_p & c_p \end{bmatrix},$$

$$\mathbf{K} = \begin{bmatrix} k_s + k_p & -k_p \\ -k_p & k_p \end{bmatrix},\ \mathbf{q} = \begin{bmatrix} x_s \\ x_p \end{bmatrix},\ \mathbf{f} = \begin{bmatrix} u \\ 0 \end{bmatrix} \qquad (10)$$

The nonlinear state equations $\mathbf{f(x)}$ can then be linearized to $\mathbf{Ax}$, where,

$$\mathbf{A} = \begin{bmatrix} \mathbf{0} & \mathbf{I} \\ -\mathbf{M}^{-1}\mathbf{K} & -\mathbf{M}^{-1}\mathbf{C} \end{bmatrix} \qquad (11)$$

By setting u to zero and using the control signal v as the input, the open-loop input-output transfer function $G_s(j\omega)$ is obtained by applying Eq. (11) to Eq. (4) and taking the Fourier transform,

$$G_s(j\omega) = \mathbf{C_v}(j\omega\mathbf{I} - \mathbf{A})^{-1}\mathbf{B_v} \qquad (12)$$

To assess the stability of the linearized closed-loop system, the Nyquist plot $-hG_s(j\omega)$ is shown in Figure 2 using the parameters in Table 1 and a control gain $h = 20$. Here, it is apparent that the system is conditionally stable at 9.8 Hz; increasing the control gain will eventually result in the locus encircling the (-1, 0) point, thereby destabilizing the closed-loop system. This particular frequency corresponds to the peak resonance frequency of the actuator when attached to the flexible structure.

Table 1. Parameter values.

Parameter	Value
m_s	0.05 kg
c_s	0.32 Ns/m
k_s	5000 N/m
m_p	0.032 kg
c_p	1.3 Ns/m
k_p	124 N/m
k_{sat}	1.3 x 10^6 N/m
d	1 mm

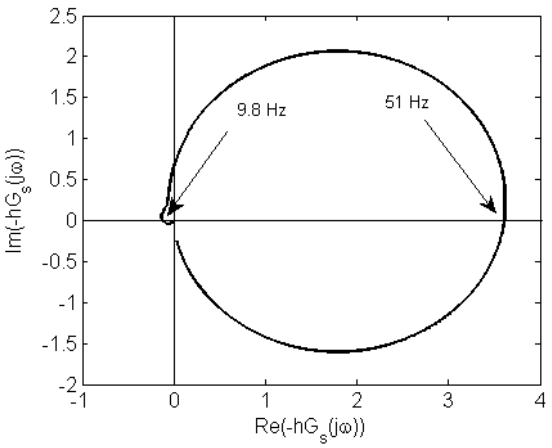

Figure 2. Nyquist plot of the linearized system.

The maximum stable feedback gain h_s of the closed-loop system is obtained from the Nyquist plot as,

$$h_s = \frac{20}{0.1186} \approx 168 \qquad (13)$$

Thus, the linearized system is stable if $h < h_s$. This gain margin is relatively large, and so it should be possible to implement a reasonable increase in the effective structural damping that is well within the stability limits.

However, if the relative displacement between the proof-mass and the structural mass is sufficiently large, the actuator becomes stroke-saturated, and $h < h_s$ is no longer a sufficient condition for global closed-loop stability. This is apparent from the presence of limit-cycle oscillations observed in the closed-loop dynamics, even if h is well below the linear stability threshold h_s. As an example, the absolute and relative displacement-time histories of the structural mass and proof-mass, as specified in Table 1, are simulated using MATLAB's ode45 solver, as shown in Figure 3. The structural mass is excited by a 20 N impulse, with a duration of 5 milliseconds, and the control gain is $h = 10$. Here, it can be seen that the closed-loop system is unstable, and that the relative displacement enters a limit-cycle oscillation.

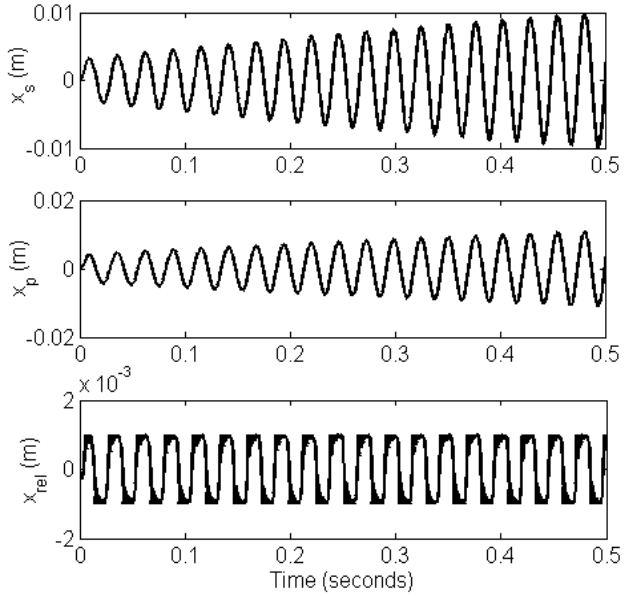

Figure 3. Time series depicting the displacement responses of the proof-mass and the structure.

A crude indication of the nonlinear relative closed-loop stability is obtained by approximating the state matrix $\mathbf{A}$ for a given state vector as follows,

$$\mathbf{f_c(x)} = \mathbf{A(x,}h\mathbf{)x},\quad \mathbf{A(x,}\ h\mathbf{)} = \begin{bmatrix} \mathbf{0} & \mathbf{I} \\ -\mathbf{M}^{-1}\mathbf{K_{tot}} & -\mathbf{M}^{-1}\mathbf{C_h} \end{bmatrix} \qquad (14)$$

where,

$$\mathbf{K_{tot}} = \begin{bmatrix} k_s + k_{tot}(x_s, x_p) & -k_{tot}(x_s, x_p) \\ -k_{tot}(x_s, x_p) & k_{tot}(x_s, x_p) \end{bmatrix}$$

$$\mathbf{C_h} = \mathbf{C} + \begin{bmatrix} gh & 0 \\ -gh & 0 \end{bmatrix}$$

$$k_{tot}(x_s, x_p) = k_p + k_{sat} x_{sat}, \quad x_{sat} = (1 - d/|x_{rel}|) \tag{15}$$

The eigenvalues of $\mathbf{A(x,\ h)}$, denoted as $\lambda_i(x_{rel}, h)$, are then ascertained over different values of x_{rel} and h, and the real part is analysed to ensure that the stability criterion $\mathrm{Re}\{\lambda_i(x_{rel}, h)\} < 0$ is satisfied. An illustration of these eigenvalues, as shown in Figure 4, reveals that the real part increases abruptly once the stroke limit d is exceeded. This phenomenon becomes more pronounced as h increases, such that the real part of the eigenvalues becomes positive around the stroke limit for control gains as small as small as $h = 10$. In this case, the closed-loop system may become unstable and enter a limit-cycle oscillation, as illustrated in Figure 3.

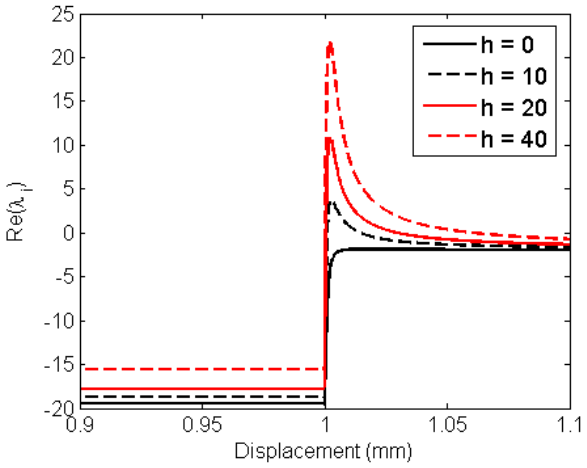

Figure 4. Real part of eigenvalues λ_i against x_{rel} and h.

Clearly, stroke saturation is highly detrimental to the closed-loop stability margin, which is reduced by an approximate factor of 17.

3 LYAPUNOV ENERGY ANALYSIS

In order to minimize the effect of stroke saturation on the closed-loop stability margin, it is necessary to consider the underlying physical behaviour of the system, such that an appropriate control law can be devised. For this purpose, we utilize Lyapunov's direct method [9] to assess the closed-loop stability and to identify the physical causes of destabilization. Here, the total mechanical energy E is chosen as the basis of the Lyapunov function $V(\mathbf{x})$ to provide physical intuition. The total mechanical energy is the sum of the structural kinetic energy T_s, the proof-mass kinetic energy T_p, and the total potential energy U. From Eq. (4), the appropriate expressions for these terms are,

$$T_s = \frac{1}{2} m_s \dot{x}_s^2 \tag{16}$$

$$T_p = \frac{1}{2} m_p \dot{x}_p^2 \tag{17}$$

$$U = \begin{cases} \frac{1}{2}(k_s x_s^2 + k_p x_{rel}^2 + k_{sat}(x_{rel} - d)^2) & |x_{rel}| > d \\ \frac{1}{2}(k_s x_s^2 + k_p x_{rel}^2) & |x_{rel}| < d \end{cases} \tag{18}$$

The Lyapunov function is then defined in the quadratic format $V(\mathbf{x}) = \mathbf{x}^T \mathbf{P} \mathbf{x}$, where,

$$\mathbf{P} = \frac{\begin{bmatrix} \mathbf{K_V(x)} & 0 \\ 0 & \mathbf{M} \end{bmatrix}}{2}$$

$$\mathbf{K_V(x)} = \begin{cases} \mathbf{K} + \begin{bmatrix} k_{sat} x_{sat}^2 & -k_{sat} x_{sat}^2 \\ -k_{sat} x_{sat}^2 & k_{sat} x_{sat}^2 \end{bmatrix} & |x_{rel}| > d \\ \mathbf{K} & |x_{rel}| < d \end{cases} \tag{19}$$

For local asymptotic stability to be assured, the Lyapunov function must satisfy LaSalle's invariance principle [10], which can be summarised by the following conditions,

(1) $V(\mathbf{x}) = 0$ if and only if $\mathbf{x} = \mathbf{0}$
(2) $V(\mathbf{x}) > 0$ for set $S: \mathbf{x} \in \mathfrak{R}^n \rightarrow \mathfrak{R},\ \mathbf{x} \neq \mathbf{0}$
(3) $\dot{V}(\mathbf{x}) = 0$ if and only if $\mathbf{x} = 0$
(4) $\dot{V}(\mathbf{x}) < 0$ for set $S: \mathbf{x} \in \mathfrak{R}^n \rightarrow \mathfrak{R},\ \mathbf{x} \neq \mathbf{0}$

First, we consider the local stability of the linear region of the closed-loop system, with set $S: \mathbf{x} = \{\forall \mathbf{x}, |x_{rel}| < d\}$. Here, it is apparent that the set satisfies conditions (1) and (2), since $\mathbf{P}$ is positive-definite. The Lie derivative of the Lyapunov function can be expressed as,

$$\dot{V}(\mathbf{x}) = -\dot{\mathbf{q}}^T \mathbf{C_h} \dot{\mathbf{q}} \tag{20}$$

which clearly satisfies condition (3). For condition (4) to be satisfied, $\mathbf{C_h}$ should be a positive-definite matrix, which is true for the open loop. However, it is apparent from Eq. (15) that the feedback control disrupts the symmetry of $\mathbf{C_h}$, and so it is necessary to utilize Cholesky decomposition to determine the positive-definiteness of $\mathbf{C_h}$. Here, $\mathbf{C_h}$ is expressed by a lower triangular matrix $\mathbf{L_c}$ that satisfies $\mathbf{C_h} = \mathbf{L_c} \mathbf{L_c}^T$. Provided that the diagonal terms of $\mathbf{L_c}$ are non-negative, then $\mathbf{C_h}$ is positive-definite and Eq. (20) satisfies conditions (3) and (4). These diagonal terms are plotted against the feedback control gain in Figure 5. Surprisingly, one of the diagonal terms becomes negative at $h \approx 0.89$, which implies that the closed-loop system becomes unstable when $h > 0.89$. This result is inconsistent with the gain margin stated in Eq. (13), where h must exceed 168 for instability to occur.

The reason for this discrepancy is that the total mechanical energy of the system can increase with time without inducing

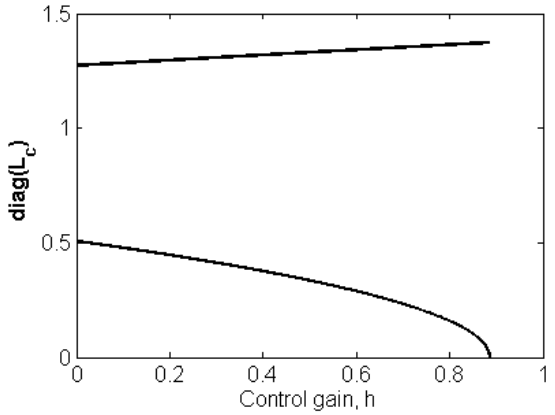

Figure 5. Diagonal terms of $\mathbf{L_c}$ against h.

closed-loop destabilization. This is illustrated in Figure 6, where the total closed-loop energy is shown against time, with an impulse excitation of 20 N and a control gain $h = 20$. Here, it is apparent that whilst the total energy decays asymptotically towards zero, the feedback control is sufficient to increase the total energy at certain times. It is believed that these regions of potential instability are caused by a large increase in the kinetic energy of the proof-mass as it moves from one side of the stroke to the other, since the feedback control amplifies the proof-mass vibrations.

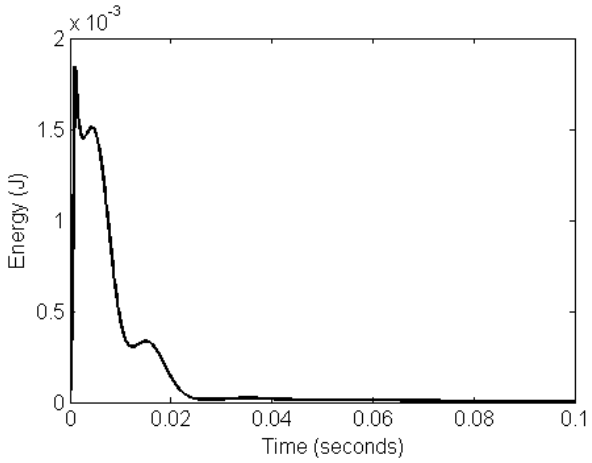

Figure 6: Total energy of the closed-loop system against time. Although the total energy decays asymptotically to zero, the feedback control increases the energy at certain times.

It is evident from this analysis that although the total mechanical energy is useful for revealing the underlying physics of the actuator-structure system, it not a suitable Lyapunov function for assessing closed-loop stability. To overcome this problem, an alternative form of the Lyapunov function is sought. First, the Lie derivative of the Lyapunov function is defined in the more generalized form,

$$\dot{V}(\mathbf{x}) = -\mathbf{x}^T\mathbf{Q}\mathbf{x} \tag{21}$$

such that $\dot{V}(\mathbf{x})$ is dependent on $\mathbf{x}$ rather than $\dot{\mathbf{q}}$. The matrix $\mathbf{Q}$ is related to $\mathbf{P}$ via the Lyapunov equation,

$$\mathbf{A}^T\mathbf{P} + \mathbf{P}\mathbf{A} = -\mathbf{Q} \tag{22}$$

It should be noted that this formularization is only valid within the linear regime of the actuator. In this case, $\mathbf{Q}$ is specified as the identity matrix $\mathbf{I}$ and $\mathbf{P}$ is obtained from Eq. (22). Since the Lyapunov function is quadratic and $\mathbf{Q}$ is negative-definite, conditions (1), (3) and (4) are satisfied. Therefore, if the $\mathbf{P}$ matrix is positive-definite, then condition (2) is satisfied and the closed-loop system is asymptotically stable. This is assessed by obtaining the eigenvalues of $\mathbf{P}$ and establishing the real part is negative. An illustration of the eigenvalues against the feedback control gain, as shown in Figure 6, indicates that $\mathbf{P}$ is positive-definite up to $h \approx 168$, which is consistent with Eq. (13).

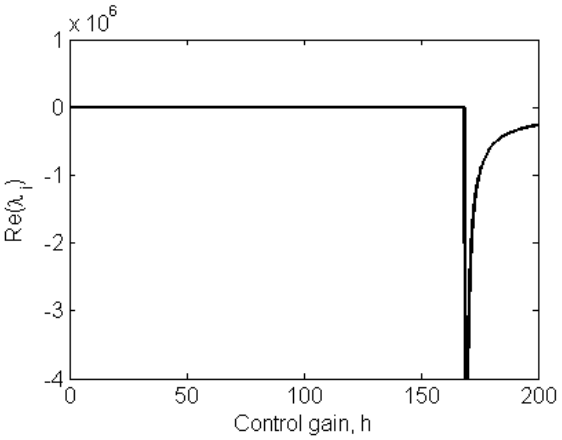

Figure 7: Eigenvalues of $\mathbf{P}$ against h.

Now that it has been established that the closed-loop system is locally stable if $h < 168$, the global closed-loop stability is assessed, with no restrictions on $\mathbf{x}$. Here, the effects of stroke saturation are accounted for using the general Lyapunov function in Eq. (19). The Lie derivative is specified in Eq. (20), such that the regions of potential instability observed in Figure 5 remain present. However, whilst the regions of potential instability are not sufficient to destabilize the closed-loop system in the linear regime, they have a significant effect whenever stroke saturation occurs. This is apparent in Figure 8, which illustrates the total mechanical energy of the closed-loop system, accounting for stroke saturation. In this case, the total energy increases over time, resulting in a limit-cycle oscillation.

To further investigate the underlying physics of the actuator-structure configuration, the energy curve shown in Figure 8 is sub-divided into the energy groups defined in Eqs. (16-18). By analysing these individual contributions, as shown in Figure 8, it is evident that there are several features of interest. Firstly, the stroke saturation phenomenon has the initial effect of reducing the total energy of the system, which is mostly transferred as kinetic energy to the structural mass. Secondly, the total potential energy rises to a maximum once the impulses associated with stroke saturation have decayed. Thirdly, the increase in the total energy E can be attributed to

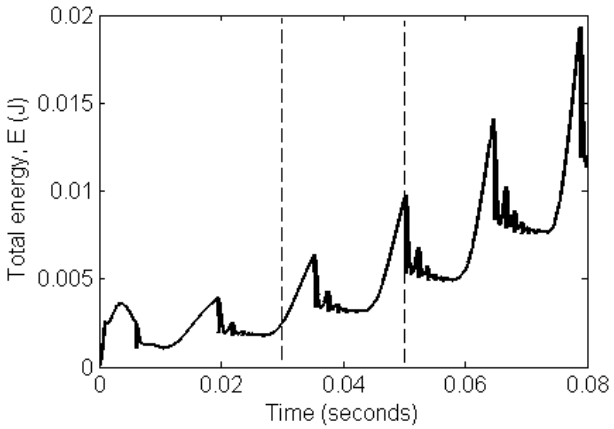

Figure 8. Total energy of the closed-loop system, in response to a 20 N impulse. The control gain is $h = 20$.

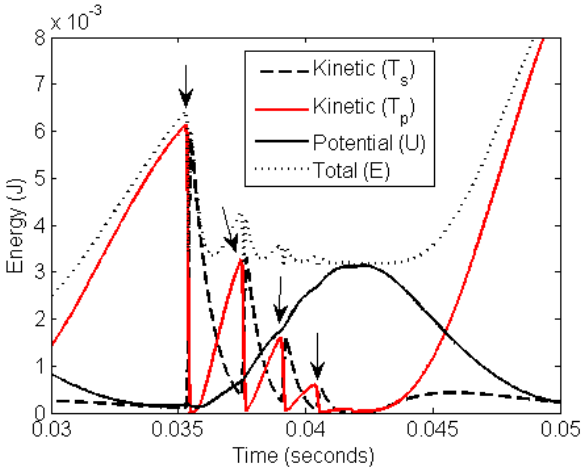

Figure 9. Contributions of proof-mass kinetic energy T_s, structural energy T_p and potential energy U to the total energy E in Figure 8 over a restricted period of time.

the kinetic energy of the proof-mass, as with the linear case. Therefore, we can determine from this analysis that stroke saturation destabilizes the closed-loop by accentuating potential instabilities that are already present in the underlying linear system. Furthermore, instability only occurs once the proof-mass has undergone stroke saturation, as indicted by the arrows in Figure 9, and, with the aid of the control signal, moves rapidly from one end stop to the other. This needs to be taken into account when considering a control strategy, which is discussed in the next section.

In order to establish a link between stroke saturation and the accentuation of the instability regions, it is necessary to examine the total potential energy of the closed-loop system. Since stroke saturation is modelled as a series of purely elastic collisions, the maximum potential energy during each cycle is greater than that of the underlying linear system, as demonstrated in Figure 10.

In addition, Figure 9 shows that the potential energy is converted into the kinetic energy of the proof-mass once the collisions have subsided. Therefore, the increased levels of potential energy due to stroke saturation results in the accentuation of the instability regions caused by the kinetic energy of the proof-mass, in conjunction with the feedback control. This describes the sequence of events that lead to the destabilization of the closed-loop system.

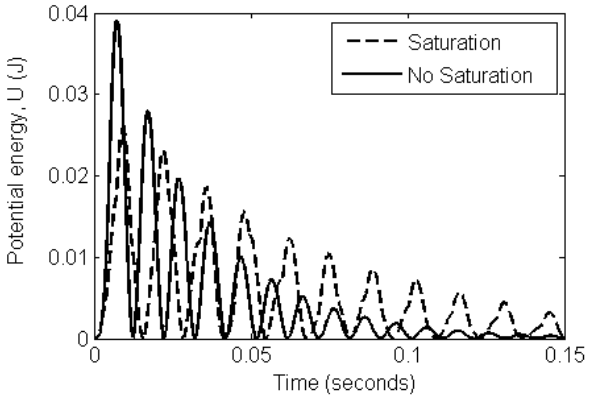

Figure 10. Potential energy of the open-loop system, with and without stroke saturation.

By considering other common types of actuator nonlinearities, such as an amplitude-dependent suspension stiffness, it can be seen that the issue of destabilization is not limited to stroke saturation; any type of hardening nonlinearity that increases the potential energy is capable of inducing instability in the closed-loop system. Therefore, these findings confirm that weak nonlinearities in a dynamic system have the potential to detrimentally affect the stability margin of the closed-loop system, and can invalidate the predictions made using linear Nyquist theory.

4 CONTROL STRATEGY SIMULATIONS

From the analysis of the previous section, it is apparent that stroke saturation, in conjunction with the feedback control, destabilizes the closed-loop system by increasing the potential energy, which in turn increases the kinetic energy of the proof mass. Since the open-loop system is globally asymptotically stable, one of the simplest possible control strategies, in principle, is to switch off the feedback control at critical moments in each cycle, such that the increase in T_p is prevented. This strategy is a variation of on-off control [11], and is advantageous for increasing the closed-loop stability margin whilst retaining good control performance in the linear regime. However, the implementation of this control strategy requires careful consideration if these objectives are to be achieved.

First, it is necessary to detect the onset of stroke saturation in the displacement-time signals, such that the feedback control can be switched off to counteract the destabilizing effects. This could be accomplished, for example, by placing an accelerometer on the actuator casing and examining the resulting signal for large, abrupt variations that represent the impacts associated with stroke saturation. To remove the contributions of higher-order modes within the frequency range of the impacts, the control signal should be low-pass filtered before being applied to the actuator. In addition, it is necessary to band-pass filter the accelerometer signal to prevent aliasing and to remove the intended low-frequency control signal from the detection process. For these purposes,

two 10^{th} order Butterworth low-pass and band-pass filters were utilized in this simulation, with a cut-off frequency of 10 k-rad/s for the low-pass filter and a bandwidth of 10 k-rad/s to 100 k-rad/s for the band-pass filter. A simple detection threshold can then be set up for the remaining high-frequency impacts in the signal.

The next step is to ensure that once stroke saturation is detected, the feedback control is switched off at suitable moments in time to prevent T_p from increasing. This presents a number of challenges. Firstly, stroke saturation comprises multiple transient impacts, which results in chattering as the signal moves from one impact to the next. Secondly, the deactivation of the feedback control should be aligned with potential increases in T_p, and it is therefore inappropriate to directly switch off the control signal during stoke saturation. Thirdly, the duration of the feedback control deactivation should depend on the time taken for the proof-mass to move from one end stop to the other, as opposed to the duration of the stroke saturation phenomenon.

To overcome these difficulties, the accelerometer signal is "held" for a user-defined length of time τ once the detection threshold is exceeded, and a delay φ is then applied to aid synchronization. This results in an "on-off" detection signal that is zero if the control is on and unity if the control is off. The choice of τ is a trade-off between control performance and closed-loop stability; the larger the value of τ, the longer the time that feedback control is switched off, resulting in greater assurance of closed-loop stability at the expense of worsening the control performance in the linear regime. Therefore, the smallest possible value of τ that assures closed-loop stability up to the linear Nyquist threshold should be chosen. Figure 10 illustrates the effect of different values of τ on the detection signal.

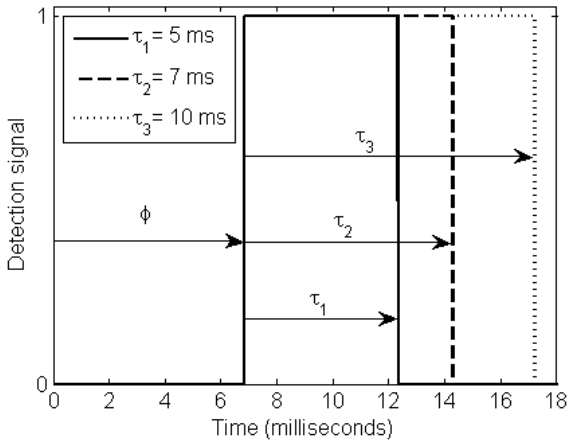

Figure 10. Detection signal for three different values of τ after detection at t = 0. For the sake of illustration, φ is set to be 7 milliseconds.

In this case, τ is defined as $\tau = 7$ milliseconds as a compromise between performance and stability.

Since the increases in T_p occur a short time t_s after the onset of stroke saturation, it is necessary to apply a delay φ to synchronize the detection signal with these increases. The time period t_s varies with each cycle, and therefore it is not possible to achieve true alignment for the detection signal using a constant delay time. Nevertheless, an approximation of the ideal delay time can be accomplished by examining the total energy of the closed-loop system and establishing what value of φ results in the fastest decay time. This is shown in Figure 11 for a control gain $h = 100$, an excitation impulse of 20 N, and a variety of delay times. The delay $\varphi = 5\,\text{ms}$ is chosen as the best parameter value for stabilizing the closed-loop system In addition, the relative displacement is shown in relation to the appropriate detection signal in Figure 12.

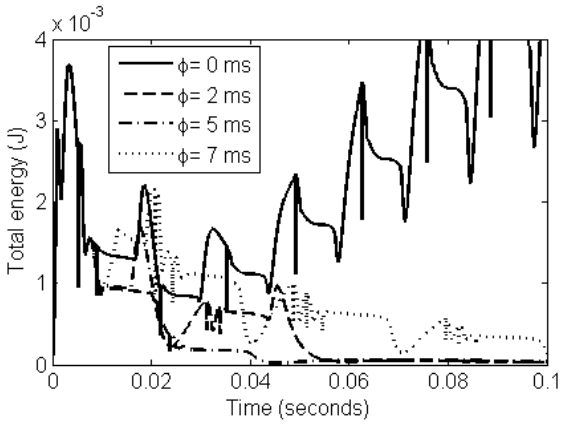

Figure 11. Total energy of the closed-loop system with on-off control. If no delay is applied to the detection signal, the system is unstable, whereas a 5 millisecond delay results in a stable system with a fast decay time.

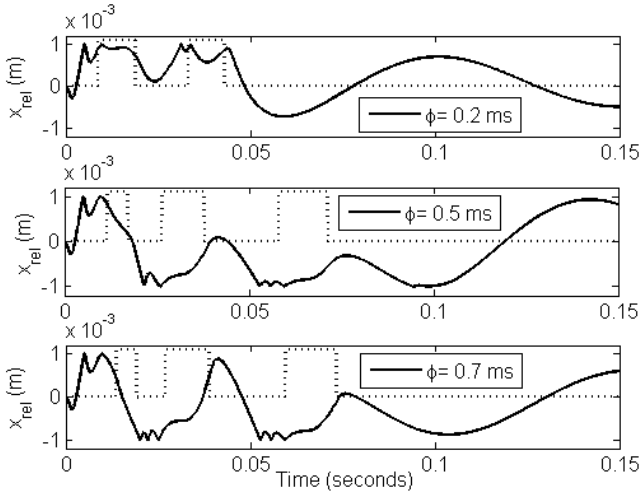

Figure 12. Synchronization of the detection signal (dashed line) with the relative displacement (solid line). Whereas a delay of 2 milliseconds results in control deactivation during stroke saturation, a delay of 5 or 7 milliseconds results in control deactivation whilst the proof-mass moves from one end stop to the other, as intended.

In order to demonstrate that the closed-loop system remains stable near the linear Nyquist threshold, two examples are illustrated in Figure 13, which shows a comparison of the

relative displacement-time signals obtained using on-off control and conventional velocity feedback control respectively. The first example features a relatively large control gain $h = 150$ and an excitation amplitude of 50 N, whereas in the second example, the control gain $h = 165$ is very close to the linear Nyquist threshold, and a smaller excitation amplitude of 40 N is utilized. Here, it is apparent that the conventional velocity feedback control results in an unstable system and a limit-cycle oscillation, whereas the on-off control is able to stabilize the closed-loop system.

It should be noted that the methods used to implement the on-off control are fairly crude and based on little more than the trial-and-error of the time parameters. However, they are sufficient for demonstrating that on-off control has the potential to prevent stroke saturation destabilizing the closed-loop system.

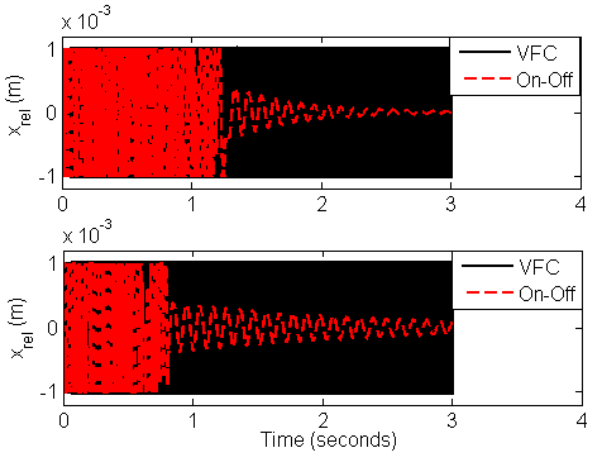

Figure 13. Relative displacement of the closed-loop system using conventional velocity feedback control (VFC) and on-off control. In the two examples described in the text, the VFC results in a limit-cycle oscillation, whereas the on-off control ensures the relative displacement decays asymptotically to zero.

To summarize, the application of on-off control is perhaps best suited to inherently linear or weakly nonlinear systems that are only occasionally subjected to large disturbances. In this case, the controller can perform as intended in the linear regime, whilst the closed-loop system remains stable when large disturbances occur. However, on-off control may not be suited to systems that regularly feature large excitation amplitudes that need to be controlled, since the controller emphasizes closed-loop stability rather than control performance. Furthermore, the dynamics of a closed-loop system with on-off feedback control are extremely complex, and it is difficult to develop a rigorous proof of closed-loop stability. To overcome these problems, additional control strategies, such as including the relative or structural displacement in the control signal, should also be considered.

5 CONCLUSIONS

This paper presents an analysis on the stability of a stroke-saturated actuator when coupled to a flexible structure. Whilst the underlying linear system is conditionally stable, accounting for stroke saturation greatly reduces the closed-loop stability margin, resulting in limit-cycle oscillations. It was found that the total energy of the closed-loop system increases with the kinetic energy of the proof-mass when it moves from one end stop to the other, with the aid of the feedback control. The resulting regions of potential instability have little effect for the underlying linear closed-loop system. However, the increased potential energy levels associated with stroke saturation are sufficient to destabilize the closed-loop system through these instability regions.

A simple on-off controller was considered for the purpose of stabilizing the closed-loop system when stroke saturation occurs. It was found that by carefully choosing the hold time and delay time of the stroke saturation detection signal, the control is deactivated as the kinetic energy of the proof-mass increases, thereby stabilizing the closed-loop system.

Future work will involve utilizing a more rigorous approach to prove that on-off control can stabilize the closed-loop system, and comparing the on-off control with other possible nonlinear controllers with regards to simplicity, stability, and performance.

ACKNOWLEDGMENTS

Laurence Wilmshurst's Ph.D is sponsored by a Rayleigh scholarship at the University of Southampton.

REFERENCES

[1] D. A. Wagg and S. Neild, *Nonlinear vibrations with control: for flexible and adaptive structures*, Springer, New York, 2010

[2] J. G. Chase, M. Yim, A. A. Berlin, Integrated centering control of inertially actuated systems, *Control Engineering Practice*, 7(9), 1999, 1079-1084

[3] D. K. Lindner, G. A. Zvonar, D. Borojevic, Performance and control of proof-mass actuators accounting for stroke saturation, *Journal of Guidance, Control, and Dynamics*, 17(5), 1994, 1103-1108

[4] O. N. Baumann, S. J. Elliott, Destabilization of velocity feedback controllers with stroke limited inertial *actuators*, *Journal of the Acoustical Society of America*, 121(5), 2007, 211-217

[5] J. G. Chase, H. A. Smith, Robust H_∞ control considering actuator saturation i: theory, *Journal of Engineering Mechanics*, 122(10), 1996, 976-983

[6] O. N. Baumann, S. J. Elliott, The stability of decentralized multichannel velocity feedback controllers using inertial actuators, *The Journal of the Acoustical Society of America*, 121, 2007, 188

[7] L. I. Wilmshurst, M. Ghandchi Tehrani, S. J. Elliott, Nonlinear vibrations of a stroke-saturated inertial actuator, *11th International Conference on Recent Advances in Structural Dynamics*, 2013

[8] Micromega Dynamic: Active Damping Devices and Inertial Actuators, http://www.micromega-dynamics.com/doc/ADD_Catalog_Rev2.pdf

[9] A. Bacciotti, L. Rosier, *Liapunov functions and stability in control theory*, Springer, 2005

[10] J. P. LaSalle, S. Lefschetz, *Stability by Liapunov's Direct Method*, Academic Press, London, 1961

[11] F. L. Lewis, *Applied Optimal Control and Estimation*, Prentice-Hall, 1992